International Journal of Heat and Mass Transfer 52 (2009) 328–336

Contents lists available at ScienceDirect

International Journal of Heat and Mass Transfer

journal homepage: www.elsevier.com/locate/ijhmt

# Loss characteristics and flow rectification property of diffuser valves for micropump applications

Yi-Chun Wang *, Jui-Cheng Hsu, Ping-Chi Kuo, Yung-Chun Lee

*Department of Mechanical Engineering, National Cheng Kung University, Tainan 70101, Taiwan*

ARTICLE INFO

*Article history:*
Received 5 September 2007
Received in revised form 21 March 2008
Available online 24 July 2008

*Keywords:*
Flat-walled diffuser
Pressure loss coefficient
Diffuser efficiency

ABSTRACT

The primary motivation for this work is to provide data on the loss characteristics and flow rectification performance of flat-walled microdiffuser valves for Reynolds numbers between 100 and 2000 which is considered deficient in literature. The diffusers are designed with a fixed slenderness of 15 and an aspect ratio of 0.92 and with diverging angles ranging from 4° to 120°. The total pressure loss coefficient of the diffuser flow is determined experimentally. Components of the loss are studied in detail by numerical simulations. Results from the computations are in satisfactory agreement with the measurements. Simulations are also carried out for nozzle flows. Based on the experimental and the computational results, efficiencies of the diffuser valves are calculated. It is shown that, for laminar flows, global flow separation plays a significant role in reducing the loss of the diffuser. Consequently, the diffuser angle corresponding to the optimum diffuser efficiency varies from 40° at $Re = 100$ to 20° for $Re \geqslant 500$.

© 2008 Elsevier Ltd. All rights reserved.

## 1. Introduction

In 1993, Stemme and Stemme [1] designed and tested a valveless micropump based on the flow rectification property of diffusers. Since then much progress has been made in understanding the working characteristics and the modeling of this kind of pump [2–9]. Diffuser micropumps are of particular interest for microfluidic applications because of their simple configurations (and therefore low fabrication costs). The absence of moving structures in the fixed-geometry 'diffuser valve' eliminates the risks of valve wear and fatigue and is advantageous when the working fluid contains cells or particles prone to clogging. Moreover, in spite of the relatively low flow-directing efficiency of the diffuser, the working frequency of the diffuser micropump is generally more than one order higher than that of the passive check-valve pump of comparable size [1,2,10] and, therefore, results in much larger pump flow rate. This is especially attractive to microelectronic cooling which is highly demanding with respect to flow rate.

Many analyses and experiments have shown that the performance of diffuser micropumps is determined by the geometric design of the diffuser valve [1,2,11–16]. A workable diffuser valve is the one which has a lower pressure loss coefficient in the direction of the diffuser flow than in the nozzle flow. The ratio of the latter to the former is defined as diffuser efficiency, which must be greater than one in order to have a net pumping action. To achieve the best pump performance the diffuser efficiency should be as high as possible. Nevertheless, the design of the diffuser for micropump applications is short of solid foundation due to a lack of relevant experimental data and good analytical expressions for the pressure loss characteristics in the low Reynolds number flow regime. Indeed, all the pressure loss analyses used for designing the diffuser valve have been based mainly on the empirical data obtained at Reynolds number higher than 30,000 [17,18]. However, the maximum Reynolds number of most diffuser micropumps ranges from O(10) to O($10^3$) [1,2,10,12,13,19]. The analyses of Jiang et al. [16] showed that the loss coefficient and the efficiency of conical diffusers exhibit very different trends with diverging angle at very low (<50) and high (>$10^5$) Reynolds number ranges. More recently, Rosa and Pinho [20] demonstrated that the often-quoted expressions for the diffuser loss coefficient from the literature are only valid for turbulent flows and may lead to significant errors when flows are laminar.

Different diffuser geometries have been used for valveless micropumps. Among these are conical [1], pyramidal [4,5,14] and flat-walled [2,6,11–14]. The choice of diffuser shape is basically dependent on the fabrication process. For planar lithography and standard micromachining fabrication techniques, flat-walled diffusers (or so called the planar diffusers) are the best fit. The planar configuration widens the spectrum of possible materials and pump driver designs [2,21–26]; in addition to precision milling of metals and etching of silicon one can also apply thermoplastic molding or replication and powder blasting technique to plastics. The increasing use of plastics is foreseeable because of its low cost and good biocompatibility and chemical resistance. Another potential advantage of the flat-walled diffuser is that, under the same inlet

* Corresponding author. Tel.: +886 6 275 7575x62125; fax: +886 6 235 2973.
*E-mail address:* wangyc@mail.ncku.edu.tw (Y.-C. Wang).

0017-9310/$ - see front matter © 2008 Elsevier Ltd. All rights reserved.
doi:10.1016/j.ijheatmasstransfer.2008.06.010

**Nomenclature**

| | |
|---|---|
| $A$ | cross-sectional area |
| $d$ | hydraulic diameter |
| $g$ | gravitational acceleration |
| $h$ | elevation of tank-free surface |
| $H$ | depth of flat-walled diffuser |
| $K$ | pressure loss coefficient |
| $L$ | length of diffuser |
| $p$ | hydrostatic pressure |
| $Q$ | volumetric flow rate |
| $r_1$ | radius of rounded entrance |
| Re | Reynolds number |
| $u$ | axial velocity |
| $\overline{V}$ | volume–average velocity |
| $W$ | width of flat-walled diffuser |

*Greek symbols*

| | |
|---|---|
| $\alpha$ | kinetic-energy correction factor |
| $\varepsilon$ | pump stroke efficiency |
| $\eta_{nd}$ | diffuser efficiency |
| $\theta$ | diverging angle of diffuser |
| $\rho$ | water density |
| $\xi$ | total pressure loss coefficient |
| $\Delta p$ | frictional pressure loss |

*Subscripts*

| | |
|---|---|
| a | atmosphere |
| c | chamber |
| d | diffuser, diffuser flow |
| e | exit of diffuser valve |
| i | inlet of diffuser valve |
| in | entrance |
| j | upstream |
| k | downstream |
| n | nozzle, nozzle flow |
| o | outlet port |
| out | exit |
| 1 | diffuser neck |
| 2 | diffuser outlet |

boundary-layer condition, the best flat-walled diffuser is 10–80% shorter than the best conical design [17]. Therefore, if space is limited in the pump design, the flat-walled diffuser will give the better performance. However, attention should be given to such statements which are verified experimentally only for high Reynolds number flows.

In the literature, several steady-flow measurements on flat-walled diffusers for micropump applications have been reported and are summarized (and referenced) in Table 1. The experimental data are hard to be used to optimize the diffuser design for several reasons. First, the range of the diverging angles of the tested diffusers is very limited; the selection of the tested angles was based on the results of high Reynolds number flows and, therefore, was almost in a range of small values. Second, the slenderness and the inlet aspect ratio of the reported diffusers are very scattered. It has been shown that both parameters have prominent effects on the performance of the diffuser micropump [13]. Third, in most experiments, the reported pressure loss was not contributed only by the diffuser but also by other components (such as inlet and outlet channels, sudden expansion and contraction, bends, etc.) which were not clearly described. Therefore, the reported data represent the 'total' loss of all the components instead of the loss due to the diffuser valve solely.

In the following sections, the pressure loss coefficient based on the one-dimensional theory of the diffuser/nozzle flow is first introduced. This is followed by the description of the design and fabrication of the diffuser valves. The experimental setup for measuring the diffuser loss coefficient is then presented. To better understand the flow characteristics and the flow-rectifying ability of the diffuser valve, numerical simulations are performed using a finite volume approach and are compared with experimental data. The variations of the pressure loss coefficient and the diffuse efficiency with the diffuser angle and Reynolds number are discussed before the concluding remarks.

## 2. Pressure loss coefficient of diffuser/nozzle

Referring to Fig. 1, consider an incompressible flow through a diffuser which is connected between two ducts of areas of $A_i$ and $A_e$, respectively. The inlet and outlet areas of the diffuser are denoted by $A_1$ and $A_2$, respectively. The energy equation (per unit volume of fluid) between any two neighboring cross-sectional planes can be expressed as

$$p_j + \frac{1}{2}\alpha_j \rho \overline{V}_j^2 = p_k + \frac{1}{2}\alpha_k \rho \overline{V}_k^2 + \Delta p_{j-k} \quad (1)$$

**Table 1**
Flat-walled diffusers tested in literature

| Author and year | Diverging angles | Slenderness[a] | Area ratio[b] | Inlet aspect ratio[c] | Inlet corners | Range of Reynolds number[d] | Test unit |
|---|---|---|---|---|---|---|---|
| Olsson [2] | 9.8° | 14 | 3.3 | 1 | Rounded | < 2300 | Pump |
| Olsson et al. [11][e] | 4.2° | 33 | 4.2 | 0.33 | Rounded | <170 | Pump |
| | 1.9–6.8° | 14–37 | 1.8-5.4 | 0.24–0.35 | Rounded | <110 | Diffuser |
| Jiang et al. [16][f] | 5°, 7.5°, 10° | 60 | 12.9, 18.4, 23.8 | 1.4 | n/r | <2000 | Diffuser |
| Olsson et al. [14] | 9.8° | 14 | 3.4 | 1 | Rounded | <650 | Pump |
| | 7°, 9.8°, 13° | 13.7, 18 | 2.7, 3.4, 4.1 | 1 | Rounded | <1050 | Diffuser |
| Yang et al. [27] | 10°, 40° | 10 | 2.8, 8.3 | 1.93, 1.81 | Sharp | <400 | Diffuser |
| Yamahata et al. [25] | 9.5° | 23 | 5 | 2.5 | Rounded | <280 | Diffuser |
| Xia et al. [26] | 10° | 8, 12 | 2.4, 3.1 | 0.28, 0.42 | Sharp | n/r | Diffuser |

n/r, not reported.
[a] Diffuser length/inlet width.
[b] Outlet area/inlet area.
[c] Inlet depth/inlet width.
[d] Unless stated, the Reynolds number is based on the inlet hydraulic diameter.
[e] Non-constant diffuser depth; half-oval cross section; the Reynolds number is based on the inlet depth.
[f] Non-constant diffuser depth; cross-sectional shape not reported.

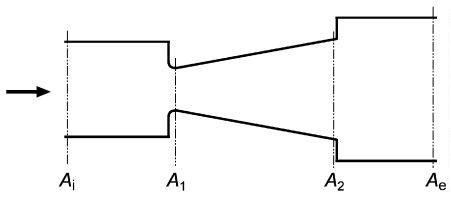


**Fig. 1.** Schematic of a diffuser flow.

in which $p$ is the (approximately uniform) hydrostatic pressure across the cross-section, $\rho$ is the (constant) fluid density, $\overline{V}$ is the volume–average velocity, the subscripts j and k represents the upstream and downstream locations, respectively, $\alpha$ is the kinetic-energy correction factor defined as [17]

$$\alpha = \frac{1}{\overline{V}^3 A}\int_A u^3\,\mathrm{d}A \tag{2}$$

$u$ is the axial velocity of the fluid and $\Delta p_{j-k}$ is the pressure loss across the segment j–k due to (irreversible) viscous dissipation. For fully-developed laminar flow, the velocity distribution is parabolic and $\alpha$ is 2 for a circular or square tube. For a nearly uniform velocity distribution (as in a turbulent flow), $\alpha$ is close to unity. In classical fluid dynamics the loss coefficient from cross-sections $j$ to $k$ is often defined as

$$K_{j-k} = \frac{\Delta p_{j-k}}{\frac{1}{2}\rho\left[\max\left(\overline{V}_j, \overline{V}_k\right)\right]^2} \tag{3}$$

Using Eq.(1) the total pressure loss from $A_i$ to $A_e$ can be expressed as

$$\begin{aligned}\Delta p_{i-e} &= \Delta p_{i-1} + \Delta p_{1-2} + \Delta p_{2-e}\\ &= p_i - p_e + \frac{1}{2}\alpha_{d,i}\rho\overline{V}_i^2 - \frac{1}{2}\alpha_{d,e}\rho\overline{V}_e^2\end{aligned} \tag{4}$$

in which, the subscript d on the kinetic-energy correction factors refers to the diffuser flow direction. If we define the total pressure loss coefficient of the diffuser–duct combination based on the maximum dynamic pressure at the diffuser neck:

$$\xi_d = \frac{\Delta p_{i-e}}{\frac{1}{2}\rho\overline{V}_1^2} \tag{5}$$

then

$$\begin{aligned}\xi_d &= K_{i-1} + K_{1-2} + K_{2-e}\left(\frac{A_1}{A_2}\right)^2\\ &= \frac{p_i - p_e}{\frac{1}{2}\rho\overline{V}_1^2} + \alpha_{d,i}\left(\frac{A_1}{A_i}\right)^2 - \alpha_{d,e}\left(\frac{A_1}{A_e}\right)^2\end{aligned} \tag{6}$$

Note that the continuity equation $A\overline{V} = \text{const.}$ has been substituted into Eq. (6). Similarly, if the flow direction in Fig. 1 is reversed (i.e., a nozzle flow), the total loss coefficient of the nozzle–duct combination is

$$\begin{aligned}\xi_n &= \frac{\Delta p_{e-i}}{\frac{1}{2}\rho\overline{V}_1^2} = K_{1-i} + K_{2-1} + K_{e-2}\left(\frac{A_1}{A_2}\right)^2\\ &= \frac{p_e - p_i}{\frac{1}{2}\rho\overline{V}_1^2} + \alpha_{n,e}\left(\frac{A_1}{A_e}\right)^2 - \alpha_{n,i}\left(\frac{A_1}{A_i}\right)^2\end{aligned} \tag{7}$$

For micropump applications, it was shown by Stemme and Stemme [1] (see also Gerlach [5]) that the pump stroke efficiency is given by

$$\varepsilon = \frac{\left|\eta_{nd}^{1/2} - 1\right|}{\eta_{nd}^{1/2} + 1} \tag{8}$$

in which $\eta_{nd} = \xi_n/\xi_d$ is the diffuser efficiency. For a diffuser pump $\eta_{nd}$ must be greater than 1 and should be as large as possible for maximum stroke efficiency. If $\eta_{nd} < 1$, the pumping flow direction is inversed (i.e., a nozzle pump) as demonstrated by Gerlach and Wurmus [4] and Gerlach [5].

Dimensional analysis of a flat-walled diffuser shows that, for incompressible flow, the performance of the diffuser depends mainly upon Reynolds number, inlet boundary-layer blockage factor (the ratio of the effective area displaced by the inlet boundary layer to the diffuser inlet area), aspect ratio, and two of the three (dependent) geometrical parameters, namely the diverging angle, the slenderness, and the area ratio [17]. Furthermore, as pointed out by Cockrell and Markland [28], while reporting diffuser data, care must be taken to stipulate the upstream and downstream conditions of the diffuser. For industrial applications, the diffuser is often preceded and followed by a parallel length of duct (i.e., $A_i = A_1$, $A_e = A_2$ in Fig. 1). The boundary-layer blockage factor at $A_1$ depends on the relative length of the upstream duct and has marked effects on the performance of the diffuser. It has also been shown that the velocity distribution at the diffuser exit ($A_2$) is always non-uniform and the downstream duct provides a settling passage in which the kinetic energy in the distorted outflow is converted to a static pressure rise due to turbulent mixing. Therefore, at high Reynolds number, the loss for the diffuser with an outlet duct is smaller than that for the same diffuser with a free discharge and the location of $A_e$ should be chosen in such a way that $p_e$ achieves a maximum [28]. For laminar flows, however, effects of the inlet and outlet conditions on the diffuser performance are as yet unclear.

In diffuser micropumps, the diffuser is in general connected directly to a large pumping chamber and an inlet or outlet port, as shown in Fig. 2, corresponding to situations of thin inlet boundary layer at $A_1$ and a free discharge at $A_2$. Accordingly, the present study is conducted with such a diffuser–chamber combination. After taking $A_i \gg A_1$ and $A_e \gg A_2$, Eqs. (6) and (7) can be written as

$$\xi_d = K_{d,in} + K_d + K_{d,out}\left(\frac{A_1}{A_2}\right)^2 \approx \frac{p_c - p_o}{\frac{1}{2}\rho\overline{V}_1^2} \tag{9}$$

$$\xi_n = K_{n,out} + K_n + K_{n,in}\left(\frac{A_1}{A_2}\right)^2 \approx \frac{p_o - p_c}{\frac{1}{2}\rho\overline{V}_1^2} \tag{10}$$

in which $p_c$ and $p_o$ are the hydrostatic pressures in the chamber and the outlet/inlet port, respectively, $K_d = K_{1-2}$ is the loss coefficient of the diffuser, $K_n = K_{2-1}$ is that of the nozzle, $K_{d,in} = K_{i-1}$, $K_{d,out} = K_{2-e}$, $K_{n,in} = K_{e-2}$, and $K_{n,out} = K_{1-i}$, respectively, denote the entrance and exit losses of the diffuser and the nozzle. According to Eqs. (1) and (3),

$$K_d = \frac{\Delta p_{1-2}}{\frac{1}{2}\rho\overline{V}_1^2} = \frac{p_1 - p_2}{\frac{1}{2}\rho\overline{V}_1^2} + \alpha_{d,1} - \alpha_{d,2}\left(\frac{A_1}{A_2}\right)^2 \tag{11}$$

$$K_n = \frac{\Delta p_{2-1}}{\frac{1}{2}\rho\overline{V}_1^2} = \frac{p_2 - p_1}{\frac{1}{2}\rho\overline{V}_1^2} + \alpha_{n,2}\left(\frac{A_1}{A_2}\right)^2 - \alpha_{n,1} \tag{12}$$

$$K_{d,in} \approx \frac{p_c - p_1}{\frac{1}{2}\rho\overline{V}_1^2} - \alpha_{d,1}, \quad K_{d,out} \approx \frac{p_2 - p_o}{\frac{1}{2}\rho\overline{V}_2^2} + \alpha_{d,2} \tag{13}$$

$$K_{n,in} \approx \frac{p_o - p_2}{\frac{1}{2}\rho\overline{V}_2^2} - \alpha_{n,2}, \quad K_{n,out} \approx \frac{p_1 - p_c}{\frac{1}{2}\rho\overline{V}_1^2} + \alpha_{n,1} \tag{14}$$

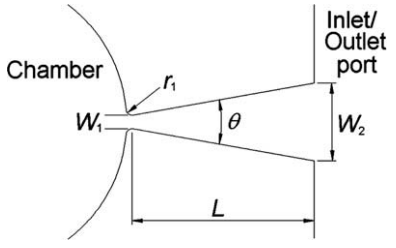


**Fig. 2.** Schematic top-view of a diffuser valve.

In the literature, the design of the diffuser valve was mainly based on the empirical data obtained in experiments at high Reynolds numbers and, therefore, might not be appropriate for low Reynolds number flows. Also, the values of $K_d$ were usually taken from the experimental data associated with diffuser–duct combination which can be very different with those of diffuser–chamber combination. Furthermore, the values of $K_{d(n),in}$ and $K_{d(n),out}$ were usually referred separately to the data associated with entrance and exit losses under the assumption that the interference between different regions of the flow shown in Fig. 1 could be neglected [11,14,25]. For example, $K_{d,out}$ was usually taken as unity with the understanding that all the kinetic energy at the diffuser exit is lost. This is correct only if $\alpha_{d,2} \approx 1$, i.e., the velocity distribution at the exit of the diffuser is nearly uniform, a situation only true for small angle diffuser at high Reynolds number. We will demonstrate that, in the low Reynolds number flows studied presently, $\alpha_{d,2}$ differs from unity and increases rapidly with the diffuser angle and Reynolds number.

## 3. Design and fabrication of microdiffusers

In order to increase the diffuser efficiency (and thus the stroke efficient of the diffuser pump), the entrance loss of the diffuser, $K_{d,in}$, should be as low as possible. For high Reynolds number flows, $K_{d,in}$ can be significantly reduced for a well-rounded entrance [17]. We do not know if it is still the case at low Reynolds number.

Fig. 3 shows the computational entrance losses associated with different edge geometries at Reynolds numbers ranging from 100 to 2000. The details of the numerical method will be described later (in Section 5). The computational domain is shown in Fig. 3(a). The relative edge radius, $r_1/d_1$, varies from 0 to 0.6. The entrance loss coefficient, $K_{in}$, is calculated from Eq. (13). As shown in Fig. 3(b), the entrance loss greatly depends upon both the entrance geometry and Reynolds number. For a given Reynolds number, the smaller the edge radius, the higher the entrance loss, however, there still exist considerable losses even for $r_1/d_1 \geqslant 0.2$, which has a nearly negligible loss ($K_{in} \leqslant 0.05$) at high Reynolds number [17]. Therefore, it would not be appropriate to use the values for the entrance loss coefficient in the literature which contains data for high Reynolds number flows only.

The chamber and the diffuser (shown in Fig. 2) are directly fabricated on a 5-mm-thick polished aluminum plate using a precision CNC milling machine. The length, $L$, of all diffusers is 9.75 mm and the diffuser inlet width, $W_1$, is fixed as 650 μm, giving a slenderness $L/W_1 = 15$. The diffuser diverging angle, $\theta$, varies from 4° to 120°, resulting in the area ratio, $A_2/A_1 = W_2/W_1$, in the range of 1.3–53. All diffusers are designed with an inlet rounded corner of $r_1 = 250$ μm. The depth of all diffusers is about $H$=600 μm, defining an inlet aspect ratio, $H/W_1$, of 0.92 and a relative entrance edge radius, $r_1/d_1$ of 0.4, where $d_1 = 624$ μm is the inlet hydraulic diameter of the diffuser.

The geometrical dimensions and wall roughness of all diffusers are measured by a 3D confocal microscope (NanoFocus μSurf™, NanoFocus AG, German) whose vertical and lateral resolutions are, respectively, 50 nm and 2.5 μm. The length, $L$, and the inlet width, $W_1$, of the diffusers fit in with the design. The depth, $H$, is

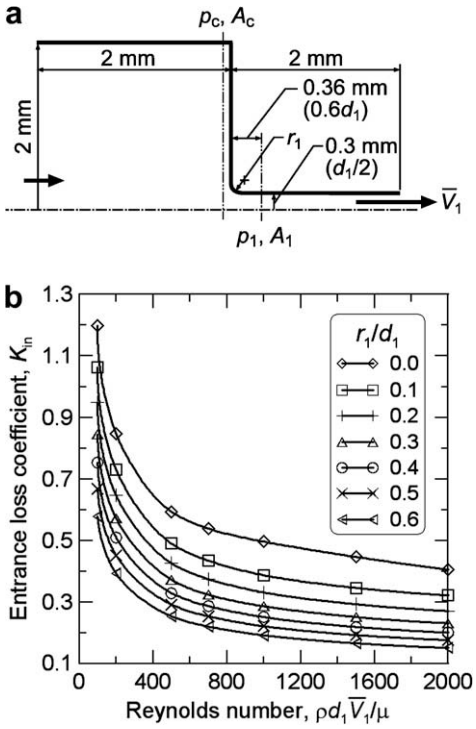


**Fig. 3.** (a) Computational domain for entrance loss calculation; (b) entrance loss coefficient as function of Reynolds number for various axisymmetric edge radii.

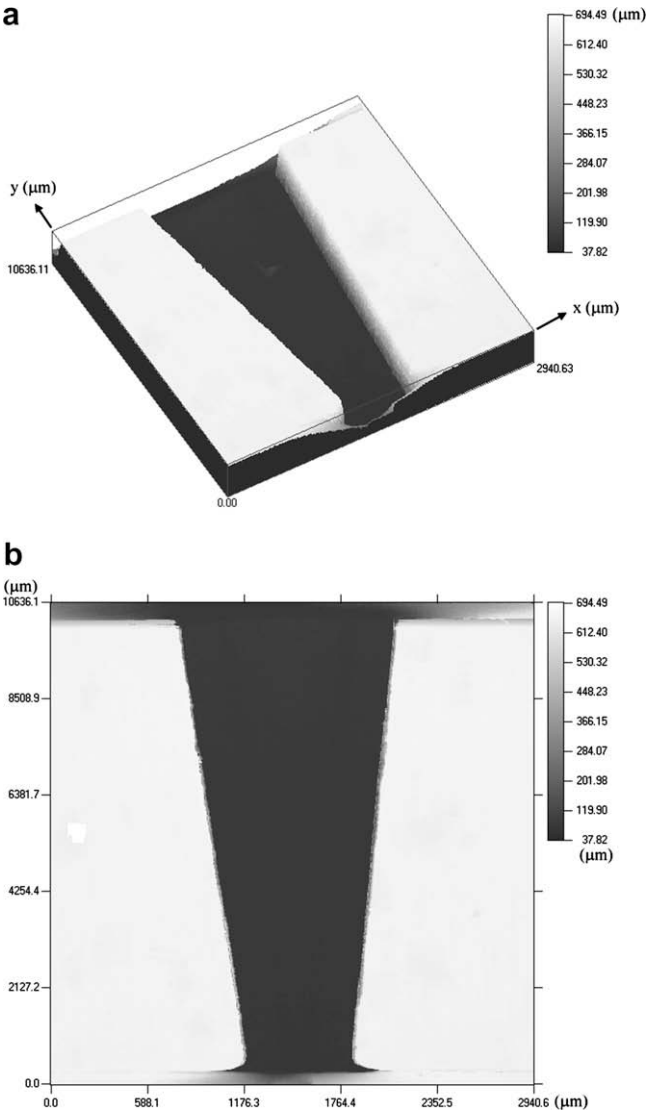


**Fig. 4.** (a) Three-dimensional and (b) top-view microscopic photographs of a 4°-diffuser. Note that the scales of the vertical ($y$) and horizontal ($x$) axes are not identical.

in the range of 600 ± 30 μm. Fig. 4 shows the 3D profile and the top view of the 4°-diffuser. The mean roughness of the diffuser surface is measured as 1.3 μm, resulting in a relative roughness of 0.2% (based on the inlet hydraulic diameter). Therefore, the diffuser wall can be considered hydraulically smooth [29].

## 4. Experimental setup

A schematic of the experimental apparatus is shown in Fig. 5. A programmable syringe pump (KDS 200, KD Scientific Inc., MA, USA) is filled with deionized water and provides a steady precision flow rate through the chamber and the diffuser. The flow rates of the pump are set as 3.675 ml/min for $Re = 100$ up to 73.5 ml/min for $Re = 2000$ (where Re is the Reynolds number based on the inlet hydraulic diameter of the diffuser). The uncertainty of the flow rate is less than ±1%. The diffuser outlet discharges directly to a large tank with a base area of 14.5 cm × 16.5 cm. The chamber pressure is measured by a high precision pressure sensor (Super TJE, Honeywell, OH, USA) with a pressure range of 0–10 psig. The uncertainty of the pressure reading is ±0.005 psi. The diffuser layer is tightly bolted between an upper cover (filmed with vacuum-sealing oil) and the base of the tank (sealed by an o-ring) to prevent any leakage.

Assuming the water is incompressible, the steady-flow energy equation between the surface of the pressure sensor (denoted by the subscript c) and the tank free surface (denoted by the subscript a) is

$$p_c + \frac{1}{2}\alpha_c \rho \overline{V}_c^2 = p_a + \frac{1}{2}\alpha_a \rho \overline{V}_a^2 + \rho g h + \Delta p_{c-a} \tag{15}$$

in which $\overline{V}_c = 0$, $\overline{V}_a \approx 0$, $\rho g h$ is the elevation pressure difference between the pressure sensor and the tank-free surface, and $\Delta p_{c-a}$ is the total pressure loss which includes the entrance loss from chamber to diffuser, the loss of the diffuser, and the exit loss from diffuser to tank. Therefore, the total loss coefficient of the diffuser–chamber combination is given by

$$\zeta_d = \frac{p_c - p_a - \rho g h}{\frac{1}{2}\rho \overline{V}_1^2} \tag{16}$$

in which $p_c - p_a$ is the gauge pressure measured by the transducer and $\overline{V}_1 = Q/(W_1 H)$ is the volumetric velocity at the diffuser neck, $Q$ is the preset volumetric flow rate of the syringe pump. Due to the large volume of the tank, the change of the elevation, $h$, during each test run is negligible.

## 5. Numerical simulations

The motivation for simulating the flows of the diffuser valves is twofold. First, the method described in the last section can only be used to measure the loss coefficient without offering any explanation for the variational trend shown in the experimental data. For example, what are the roles played by flow separation and wall friction in determining the loss coefficient and how important the entrance and exit losses are? Second, there is a clear need for establishing reliable tools in designing the diffuser valve. The numerical model can be validated by comparing with the experimental data and the accuracy of the numerics can be checked.

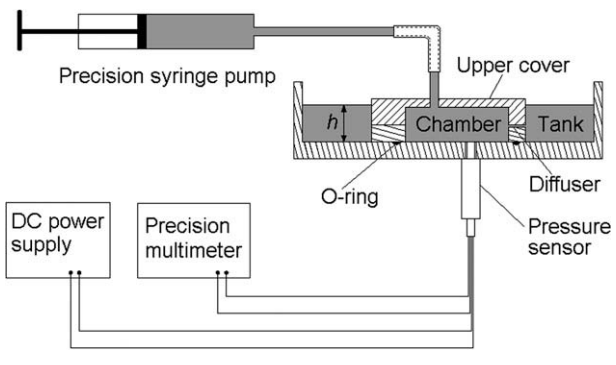


**Fig. 5.** Experimental setup.

The computational domain is based on the experimental geometry and consists of a large inlet chamber, a diffuser, and an outlet reservoir. The computational models of the diffusers are exactly the same as those described in Section 3. Due to the geometrical symmetry (which is verified using a full domain computation), only a quarter of the solution domain is modeled (by making use of symmetry boundary conditions). A uniform velocity is applied at the chamber inlet and the pressure at the outlet of the reservoir is set as zero. No-slip boundary conditions are imposed on the walls.

The flow is considered incompressible and laminar. For the range of Reynolds numbers in this study, the assumption of laminar flow seems questionable because previous experimental observations of the Reynolds number at transition from laminar to turbulent flow in micro-channels are inconsistent and contradictory. For example, Peng et al. [30] and Mala and Li [31] found early laminar-to-turbulent transition at $Re = 200$–$700$ and 600–900, respectively. However, Hetsroni et al. [29] recently reviewed and analyzed data from the literature on pressure drop in micro-channels with hydraulic diameter ranging from 1.01 μm to 4010 μm and concluded that the critical Reynolds number from Laminar-to-turbulent flow in micro-channels is consistent with the conventional theory of macro-channels. The transition from laminar-to-turbulent flow occurs at $1800 \leqslant Re \leqslant 2200$ for smooth and rough micro-channels with relative wall roughness between 0.32% and 7%. Also, in a recent publication, Kohl et al. [32] directly measured the pressure distribution along micro-channels with hydraulic diameter ranging from 25 to 100 μm and did not find any evidence of early transition. Several possible reasons for the inconsistency of the experimental data with the conventional theory were suggested by Hetsroni et al. [29] and Kohl et al. [32], including experimental uncertainties, underestimated actual roughness of the channel wall, and unaccounted entrance effects of the channel.

The simulations are carried out using the finite volume method. The commercial software package Fluent™ is used to model and solve the flows. The basic differencing schemes are central differencing for the diffusion terms and quadratic upwind interpolation for the convective terms (the QUICK scheme). The pressure–velocity coupling is based on the SIMPLE algorithm. Convergence criterion is set as that the normalized norm of the residual for each variable is less than $10^{-5}$.

Three-dimensional mixed grids are used in the present computation: structured grids for the inlet chamber and the outlet reservoir and tetrahedral unstructured grids in the region of the diffuser. The aspect ratio of the grids is controlled below 5 for good grid quality. Grid independence of the solution is checked for each case by successively refining the grids. Table 2 presents a typical example of this. Usually, it is necessary to refine the grids of the flow region in which vortices are formed to attain the convergent solution. The total numbers of grids are between 225,115 (for small-angle diffusers) and 920,290 (for large-angle diffusers).

## 6. Results and discussion

### 6.1. Comparison of experimental results and simulations

Fig. 6 presents the comparison between the experimental and computational total pressure loss coefficients of the microdiffusers. The simulations are carried out for Reynolds numbers ranging from

**Table 2**
Grid independence test for 20° diffuser at $Re = 100$

| Mesh at diffuser neck | Total grid number | Pressure loss coefficient, $\xi_d$ | Relative error[a] (%) |
|---|---|---|---|
| 6 × 6 | 90,448 | 3.1911 | 24.53 |
| 7 × 8 | 143,062 | 3.4699 | 35.41 |
| 13 × 14 | 198,503 | 2.5634 | 0.04 |
| 14 × 15 | 253,830 | 2.5625 | – |

[a] All errors are calculated relative to the data from the finest mesh.

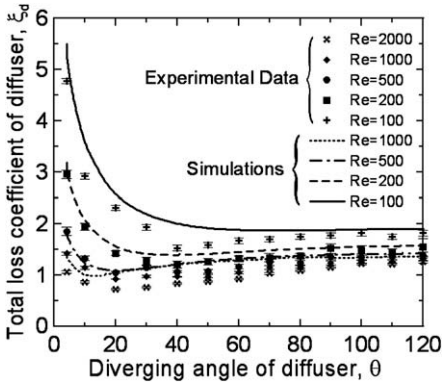


**Fig. 6.** Comparison of measured and simulated total pressure loss coefficients of microdiffusers.

100 to 1000, as for $Re = 2000$ stable solutions can not be obtained. The reason for this could be the transitional instability appearing in the flow. Fig. 6 shows that, for diffusers with very small and large diverging angles, the simulations are in satisfactory agreement with the experimental data. For medium diffuser angles, the prediction gives higher values of the diffuser loss. The average errors of the simulations are between 7% (for $Re = 200$ and 500) and 15% (for $Re = 100$ and 1000).

### 6.2. Variational trend of diffuser loss

To understand the variation of $\xi_d$ shown in Fig. 6, we plot in Fig. 7 the flow fields of diffusers with different diverging angles at $Re = 500$. Fig. 7(a) shows that, for a small diverging angle ($\theta = 10°$), there is no flow separation in the diffuser. As $\theta$ increases to 20° (Fig. 7b), separation occurs at a location about one-third of the diffuser length and forms a large circulation zone on the wall. At the same time, the loss coefficient drops down to a minimum (refer to Fig. 6). Further increase of the diverging angle leads to a forward movement of the separation point (as shown in Fig. 7c) and slightly increases $\xi_d$. For $\theta \geqslant 80°$ (Fig. 7d), separation starts immediately after the entrance and $\xi_d$ remains fairly constant thereafter. In Fig. 8, we plot together the computational total loss and the frictional force acting on the diffuser wall (obtained by integrating the wall shear stresses) for $Re = 500$. These results show that, for laminar flows, global separation helps to improve the performance of the diffuser by reducing the frictional loss on the wall and this effect becomes more prominent as Reynolds number decreases.

In Fig. 9, we compare variations of experimental total losses with Reynolds number for diffusers with small ($\theta = 4°$), medium ($\theta = 30°$), and large ($\theta = 120°$) diverging angles. Clearly the diffuser with a small diverging angle shows a strong dependence of $\xi_d$ on $Re$; the loss coefficient decreases monotonically with increasing $Re$. The loss coefficient for the small-angle diffuser at low Reynolds number is much greater than those for large-angle diffusers. Under the situation of small diverging angle the diffuser is separation-free and, therefore, the character of the relationship between $\xi_d$ and $Re$ is close to the large Moody-type loss for a straight duct. With increase in the diverging Angle, flow separation occurs at some critical Reynolds number and $\xi_d$ becomes insensitive to $Re$. The variation in $\xi_d$ at $\theta = 30°$ shows that the influence of Reynolds number is very small for $Re > 200$. For $\theta = 120°$ the flow separates directly after the smooth inlet even at $Re = 100$.

### 6.3. Loss components

The total loss of the diffuser–chamber combination, $\xi_d$, is made up of three components, namely the entrance loss, $K_{d,in}$, the diffuser loss, $K_d$, and the exit loss, $K_{d,out}(A_1/A_2)^2$ (see Eqs. 9,11, and 13). These loss components can be determined after calculating the kinetic-energy correction factors $\alpha_{d,1}$ and $\alpha_{d,2}$ by numerical integration of the velocity profiles at the inlet and the outlet planes of the diffuser respectively. Results are shown in Fig. 10. The entrance loss (Fig. 10a), $K_{d,in}$, increases appreciably when Reynolds number decreases, but is independent of the diffuser angle. On the other hand, due to the highly non-uniform velocity profile downstream of the diffuser, the exit loss is strongly influenced by the diverging angle, as shown in Fig. 10(b), in which both $K_{d,out}$

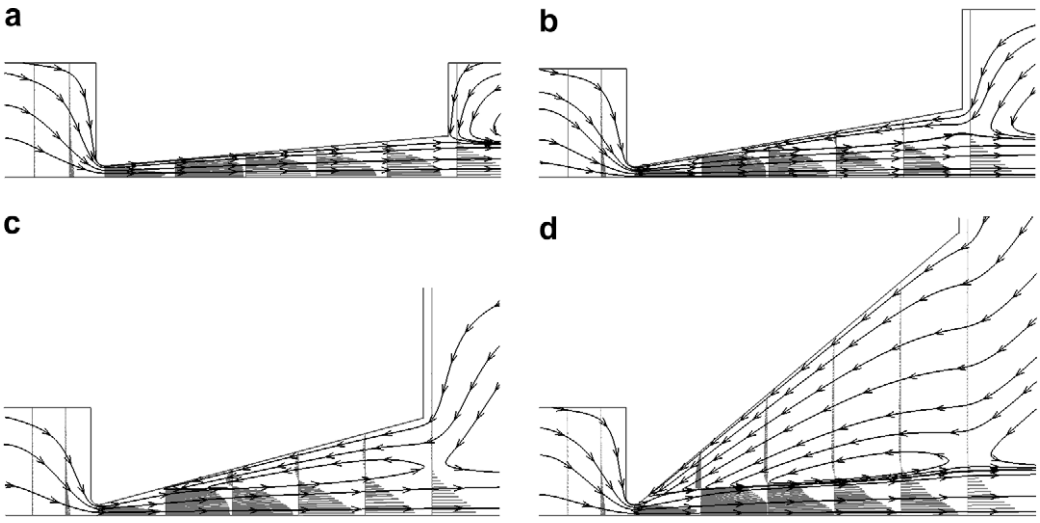


**Fig. 7.** Flow fields along symmetry axis of diffuser at $Re = 500$ for: (a) $\theta = 10°$, (b) $\theta = 20°$, (c) $\theta = 30°$, and (d) $\theta = 80°$. Velocity distributions are shown by gray lines.

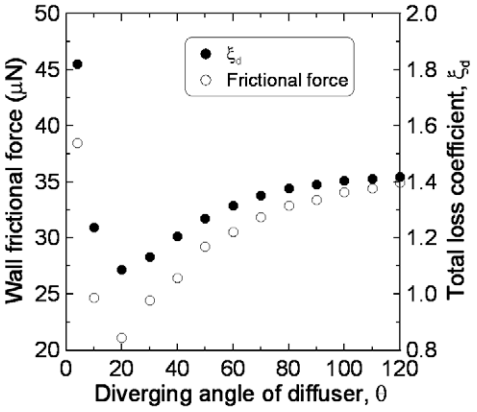


**Fig. 8.** Variations of wall frictional force and total loss coefficient with diffuser angle for $Re = 500$.

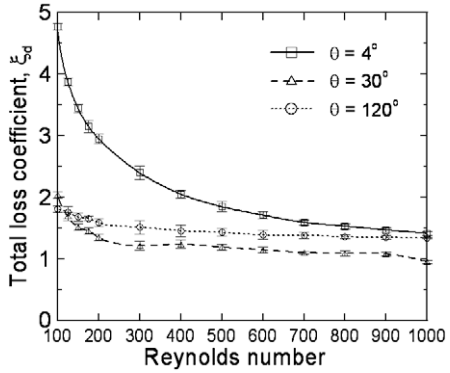


**Fig. 9.** Experimental total loss coefficient as a function of Reynolds number for small ($\theta = 4°$), medium ($\theta = 30°$), and large ($\theta = 120°$) diverging angles.

and $K_{d,out}(A_1/A_2)^2$ are plotted. The value of $K_{d,out}$ varies with Reynolds number and the diffuser angle and is very different with the common assumption for micropump analyses that $K_{d,out} = 1$ (see, for example, Olsson et al. [14]), which is only true for diffuser with separation-free (small diverging angle) and turbulent flow. In Fig. 10(b), the value of $K_{d,out}$ at $\theta = 4°$ is between 2 and 3 (approximately equal to the value of $\alpha_{d,2}$) and increases significantly with increasing diffuser angle for $Re \geqslant 200$. As an example, for $Re = 500$, the value of $K_{d,out}$ at $\theta = 50°$ is 13% higher than that for $\theta = 4°$, whereas, for $\theta = 120°$, $K_{d,out}$ is 150% greater than the value at $\theta = 4°$. At $Re = 100$, $K_{d,out}$ is less sensitive to $\theta$ and, therefore, the contribution of the exit loss, $K_{d,out}(A_1/A_2)^2$, to the total loss drops out quickly due to the fast decreasing factor of area ratio and becomes negligible for $\theta > 20°$.

Pressure loss of the diffuser, $K_d$, is shown in Fig. 10(c). For $Re = 100$ and 200, $K_d$ contributes to the major part of the total loss. As a result, the variation of $K_d$ with $\theta$ is very similar to that of $\xi_d$ (in Fig. 6). For larger Reynolds numbers ($Re = 500$ and 1000), the three loss components are equally important.

### 6.4. Flow rectification property of diffuser valve

To calculate the efficiency of the diffuser valve for micropump applications, the total loss in the nozzle direction, $\xi_n$, is required. Due to favorite pressure gradient, the nozzle flow is much simpler than the diffuser flow; no flow separation occurs in the nozzle. Therefore, the numerical solution is expected to give an accurate prediction [14]. Typical flow fields of the nozzle are shown in Figs. 11. Comparing the velocity gradients on the wall in Figs. 11(a) and (b), the small-angle nozzle has much greater wall shear stresses than the nozzle of large angle. Consequently, $\xi_n$ decreases significantly with increasing Reynolds number and the converging angle, as shown in Fig. 12.

Based on the experimental diffuser loss (plotted in Fig. 6) and the simulated nozzle loss (Fig. 12), the diffuser efficiency, $\eta_{nd} = \xi_n/\xi_d$, is calculated and given in Fig. 13. The values of $\eta_{nd}$ for all tested diffusers are between 2.04 (at $Re = 100$, $\theta = 40°$) and 0.97 (at $Re = 2000$, $\theta = 120°$). In general, diffusers with relatively small angles have a better flow rectification property than large-angle diffusers. For all Reynolds numbers, $\eta_{nd}$ first increases with increasing diffuser angle, reaches an optimum value, and then decreases substantially. The optimum diffuser angle locates at 40° for $Re = 100$ and reduces to 20° for $Re \geqslant 500$.

Despite the difficulties of directly comparing the present results with experimental data in the literature for the reasons stated near the end of Section 1, the conditions of the experiments conducted by Olsson et al. [14] are probably most close to those in our measurements. In Olsson et al. [14], flat-walled diffusers of three different diverging angles, namely 7°, 9.8°, and 13°, were tested for $Re \leqslant 1000$. The slenderness and the inlet aspect ratio of the diffusers were fixed at 13.7 and 1, respectively (see Table 1). The arithmetic mean values of the diffuser efficiency over the tested range of Reynolds number were reported as 1.59 for $\theta = 7°$, 1.43 for $\theta = 9.8°$, and 1.33 for $\theta = 13°$ [14]. By averaging $\eta_{nd}$ for Reynolds numbers between 100 and 1000 in Fig. 13, the diffuser efficiencies of the present study are found to be 1.57 for $\theta = 7°$, 1.61 for $\theta = 9.8°$, and 1.66 for $\theta = 13°$, respectively. However, attention should be given to the comments of Olsson et al. [14] that their measurements were not across only the diffuser element; some extra hydraulic components were connected to the diffuser, whose losses were estimated using the data presented in classical fluid dynamics textbooks (e.g. White [17]).

In Fig. 14, the diffuser/nozzle with diverging angle of 20° at $Re = 500$ is chosen to illustrate the influence of the diffuser depth (or aspect ratio) on the pressure loss coefficients and diffuser efficiency. The pressure loss coefficient of the nozzle, $\xi_n$, declines with the increase of the aspect ratio due to the reduction of the side-wall effect. In contrast, the loss coefficient of the diffuser, $\xi_d$, decreases initially, reaches a minimum near the aspect ratio of 1.5, and starts to increase slightly. In this chosen case, the diffuser efficiency, $\eta_{nd}$, has an optimal value at the aspect ratio of about 0.5.

## 7. Concluding remarks

This work is intended to provide information on the loss characteristics and flow rectification performance of flat-walled microdiffuser valves for valveless micropumps. Based on the experimental and the computational results, efficiencies of the diffuser valves are calculated and the following conclusions can be drawn:

1. The total pressure loss coefficient of the diffuser/nozzle decreases with increasing Reynolds number. For a fixed Reynolds number, the total loss in the diffuser is smaller than that of the nozzle except for the diffuser with a very large diverging angle, indicating that most diffuser valves in this study have flow-rectifying properties in the laminar flow regime.
2. At a given Reynolds number, a maximum diffuser efficiency is found at some specific diffuser angle, which is 40° for $Re = 100$ and reduces to 20° for $Re \geqslant 500$. At these optimal angles, the diffuser flows are found to have a minimum in the total loss.
3. Flow separation is found to play a crucial role in reducing the loss of the diffuser. For small diverging angles, no separation

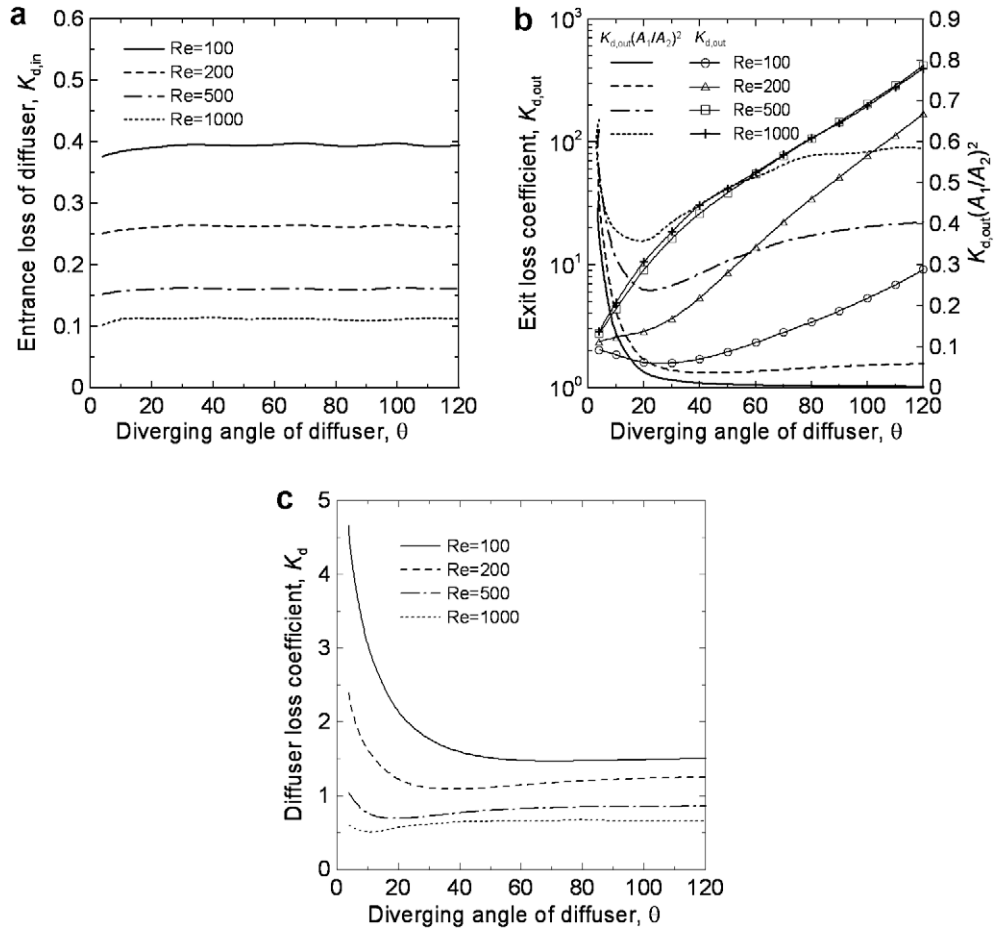


**Fig. 10.** Loss components of diffuser flow: (a) entrance loss, (b) exit Loss, and (c) diffuser loss.

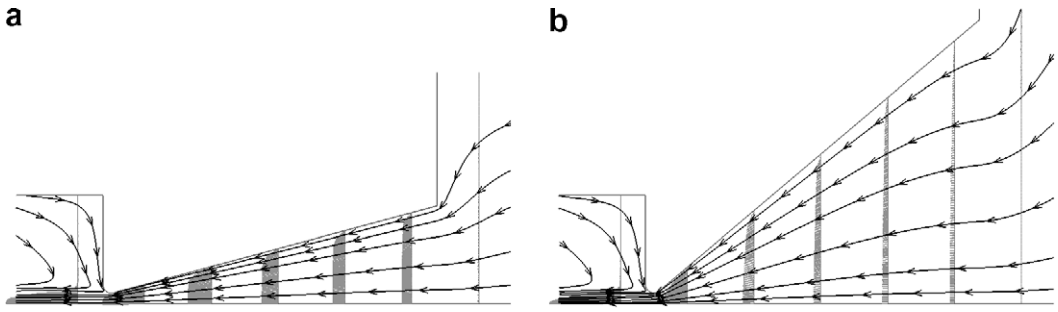


**Fig. 11.** Flow fields along symmetry axis of nozzle at $Re = 500$ for: (a) $\theta = 50°$ and (b) $\theta = 80°$. Velocity distributions are shown by gray lines.

occurs; the diffusers exhibit a large Moody-type loss. As the diverging angle increases until flow separation occurs from the frontal surface and forms a large circulation zone, the total loss of the diffuser drops down to a minimum due to a considerable reduction of wall shear stresses and becomes less sensitive to the diverging angle and Reynolds number thereafter.

4. The total loss of the diffuser value composes of three components, namely the entrance loss, the diffuser loss, and the exit loss. The entrance loss strongly depends on the entrance geometry and Reynolds number. Unlike turbulent flows, there still exists considerable loss even for a well rounded entrance. Contrary to the entrance loss, the exit loss is strongly influenced by the diverging angle due to the highly non-uniform velocity profile downstream of the diffuser. The common assumption of unity exit loss used in the literature on valveless micropumps can cause significant error.

As a closing remark, we point out that the flow in a micropump is always unsteady. In some circumstances, the unsteadiness of the flow has prominent effects on the performance of the diffuser valve. However, as demonstrated recently by Sun and Huang [33], the efficiency of a 25° microdiffuser is frequency independent for Roshko number less than 1.56. Therefore, results of the present study can be used for the design of diffuser micropumps in this quasi-steady flow regime. Of course, some micropumps can operate at exciting frequencies beyond this regime. In this case, unsteady computations/experiments must be pursued.

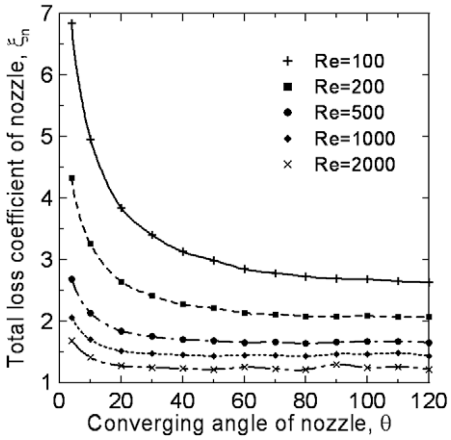


**Fig. 12.** Variation of total loss coefficient of nozzle flow with converging angle and Reynolds number.

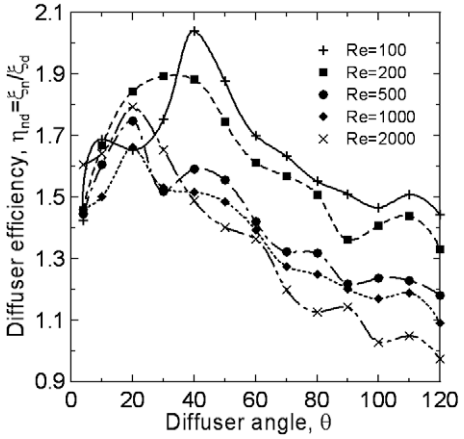


**Fig. 13.** Diffuser efficiency as functions of diffuser angle and Reynolds number.

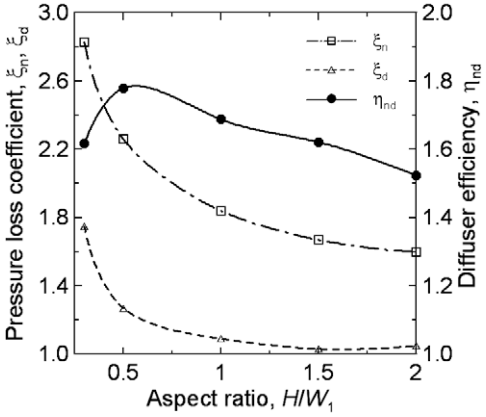


**Fig. 14.** Pressure loss coefficients and diffuser efficiency as functions of aspect ratio ($\theta = 20^\circ$ and $Re = 500$).

## Acknowledgements

The authors are grateful to the financial support from the National Science Council, Taiwan under Contract No. NSC 93-2212-E-006-060.

## References

[1] E. Stemme, G. Stemme, A valveless diffuser/nozzle fluid pump, Sensors Actuators A 39 (1993) 159–167.
[2] A. Olsson, G. Stemme, E. Stemme, A valve-less planar fluid pump with two pump chambers, Sensors Actuators A 46–47 (1995) 549–556.
[3] A. Ullmann, The piezoelectric valve-less pump – performance enhancement analysis, Sensors Actuators A 69 (1998) 97–105.
[4] T. Gerlach, H. Wurmus, Working principle and performance of the dynamic micropump, Sensors Actuators A 50 (1995) 135–140.
[5] T. Gerlach, Microdiffusers as dynamic passive valves for micropump applications, Sensors Actuators A 69 (1998) 181–191.
[6] A. Olsson, G. Stemme, E. Stemme, A numerical design study of the valveless diffuser pump using a lumped-mass model, J. Micromech. Microeng. 9 (1999) 34–44.
[7] L.S. Pan, T.Y. Ng, G.R. Liu, K.Y. Lam, T.Y. Jiang, Analytical solutions for the dynamic analysis of a valveless micropump – a fluid-membrane coupling study, Sensors Actuators A 93 (2001) 173–181.
[8] A. Ullmann, I. Fono, The piezoelectric valve-less pump-improved dynamic model, J. Microelectromech. Syst. 11 (2002) 655–664.
[9] L.S. Pan, T.Y. Ng, X.H. Wu, H.P. Lee, Analysis of valveless micropumps with inertial effects, J. Micromech. Microeng. 13 (2003) 390–399.
[10] N.-T. Nguyen, X. Huang, T.K. Chuan, MEMS-micropumps: a review, Trans. ASME J. Fluids Eng. 124 (2002) 384–392.
[11] A. Olsson, G. Stemme, E. Stemme, Diffuser-element design investigation for valve-less pumps, Sensors Actuators A 57 (1996) 137–143.
[12] A. Olsson, P. Enoksson, G. Stemme, E. Stemme, A valve-less planar pump isotropically etched in silicon, J. Micromech. Microeng. 6 (1996) 87–91.
[13] A. Olsson, P. Enoksson, G. Stemme, E. Stemme, Micromachined flat-walled valveless diffuser pumps, J. Micromech. Microeng. 6 (1997) 161–166.
[14] A. Olsson, G. Stemme, E. Stemme, Numerical and experimental studies of flat-walled diffuser elements for valve-less micropumps, Sensors Actuators A 84 (2000) 165–175.
[15] M. Heschel, M. Müllenborn, S. Bouwstra, Fabrication and characterization of truly 3-D diffuser/nozzle microstructures in silicon, J. Microelectromech. Syst. 6 (1997) 41–47.
[16] X.N. Jiang, Z.Y. Zhou, X.Y. Huang, Y. Li, Y. Yang, C.Y. Liu, Micronozzle/diffuser flow and its application in micro valveless pumps, Sensors Actuators A 70 (1998) 81–87.
[17] F.M. White, Fluid Mechanics, fourth ed., WCB/McGraw-Hill, Singapore, 1999.
[18] P.W. Runstadler, F.X. Dolan, R.C. Dean, Diffuser Data Book, Creare, New Hampshire, 1975.
[19] P. Gravesen, J. Branebjerg, O.S. Jensen, Microfluidics – a review, J. Micromech. Microeng. 3 (1993) 168–182.
[20] S. Rosa, F.T. Pinho, Pressure drop coefficient of laminar Newtonian flow in axisymmetric diffusers, Int. J. Heat Fluid Flow 27 (2006) 319–328.
[21] N.-T. Nguyen, X. Huang, Miniature valveless pumps based on printed circuit board techniques, Sensors Actuators A 88 (2001) 104–111.
[22] B. Büstgens, W. Bacher, W. Menz, W.K. Schomburg, Micropump fabricated manufactured thermoplastic molding, in: Proceedings of IEEE Micro. Electro. Mechanical Systems, Oiso, Japan, 1994, pp. 18–21.
[23] A. Olsson, O. Larsson, J. Holm, L. Lundbladh, O. Ohman, G. Stemme, Valve-less diffuser micropumps fabricated using thermoplastic replication, Sensors Actuators A 64 (1998) 63–68.
[24] C.-H. Wu, W.-C. Hsu, Fabrication of injection molded diffuser micropumps, in: Proceedings of SPIE, Micro- and Nanotechnology: Materials, Processes, Packaging, and Systems II, Sydney, Australia, vol. 5650, 2005, pp. 313–323.
[25] C. Yamahata, C. Lotto, E. Al-Assaf, M.A.M. Gijs, A PMMA valveless micropump using electromagnetic actuation, Microfluid Nanofluid 1 (2005) 197–207.
[26] F. Xia, S. Tadigadapa, Q.M. Zhang, Electroactive polymer based microfluidic pump, Sensors Actuators A 125 (2006) 346–352.
[27] K.-S. Yang, I.-Y. Chen, B.-Y. Shew, C.-C. Wang, Investigation of the flow characteristics within a micronozzle/diffuser, J. Micromech. Microeng. 14 (2004) 26–31.
[28] D.J. Cockrell, E. Markland, A review of incompressible diffuser flow, Aircraft Eng. 35 (1963) 286–292.
[29] G. Hetsroni, A. Mosyak, E. Pogrebnyak, L.P. Yarin, Fluid flow in micro-channels, Int. J. Heat Mass Transfer 48 (2005) 1982–1998.
[30] X.F. Peng, G.P. Peterson, B.X. Wang, Frictional flow characteristics of water flowing through rectangular microchannels, Exp. Heat Transfer 7 (1994) 249–264.
[31] G.M. Mala, D. Li, Flow characteristics of water in microtubes, Int. J. Heat Fluid Flow 20 (1999) 142–148.
[32] M.J. Kohl, S.I. Abdel-Khalik, S.M. Jeter, D.L. Sadowski, An experimental investigation of microchannel flow with internal pressure measurements, Int. J. Heat Mass Transfer 48 (2005) 1518–1533.
[33] C.-L. Sun, K.H. Huang, Numerical characterization of the flow rectification of dynamic microdiffusers, J. Micromech. Microeng. 16 (2006) 1331–1339.